

Isolating the Enhanced Memory of a Glassy System

Chloe W. Lindeman,^{1,*} Travis R. Jalowiec,^{2,†} and Nathan C. Keim^{2,‡}

¹*James Franck Institute and Department of Physics, University of Chicago, Chicago IL, USA*

²*Department of Physics, Pennsylvania State University, University Park, PA, USA*

(Dated: November 14, 2023)

Studies of glassy systems have shown how cyclic driving forms memories of amplitude. We explore how choice of driving protocol reveals dramatically different features of this memory. We model rearranging soft spots in sheared amorphous solids as hysterons. Cyclic shear with positive and negative shear strain reveals a return-point memory of multiple strains known from experiments and molecular dynamics simulations, while asymmetric driving (e.g. only positive shear strains) suppresses multiple memories. However, when we introduce frustrated interactions between hysterons, we identify a different mechanism that restores multiple memories for asymmetric driving and can be used for design. Our work suggests that this enhanced memory is a signature of frustration.

Asking what information a material “learns” and forgets about its past can highlight essential features of its non-equilibrium nature—traits that are often shared with another, seemingly disparate material [1]. Rubber or metal can be tested to reveal the largest strain applied previously [2, 3], hinting at the irreversible change from a single cycle of deformation. Dilute suspensions and charge-density wave conductors retain multiple amplitudes of cyclic shear [4, 5] or durations of electrical pulses [6], but lose this ability with continued driving because of irreversible change over many cycles. A ferromagnet [7] or even a system of gas molecules adsorbing onto porous glass [8] has return-point memory, which encodes a nested series of turning points of e.g. magnetic field strength or gas pressure. This type of memory, which permits the recall of multiple past amplitudes of driving, is associated with systems of reversible, hysteretic elements [7, 9]. In these and many other cases [1], one perceives a connection between the particulars of memory and key aspects of a system’s physics.

However, it is unclear whether and how this picture should extend to glassy matter. Materials such as crumpled sheets, disordered or amorphous solids, or spin ice and spin glass feature microscopic frustration wherein one relaxation inhibits another, leading to a rugged landscape of metastable states with a broad distribution of energy barriers [10]. Frustration permits behaviors that violate return-point memory [9, 11–14], and yet in several recent studies with cyclic driving, once these systems are past an initial transient they seem to show approximate or even perfect return-point behavior [15–17], most notably an amorphous solid’s memory of multiple amplitudes of shear strain [11, 18–21]. Is glassy physics relegated to perturbing known forms of amplitude memory, or does it add a distinctly glassy way of remembering?

In this Letter, we show how glassy systems can remember what non-glassy matter must forget. We consider a mesoscopic model of hysterons—elements that reversibly switch between two states, often used to represent structural rearrangements at soft spots [24–27] when an amorphous solid is deformed (Fig. 1). An ensemble

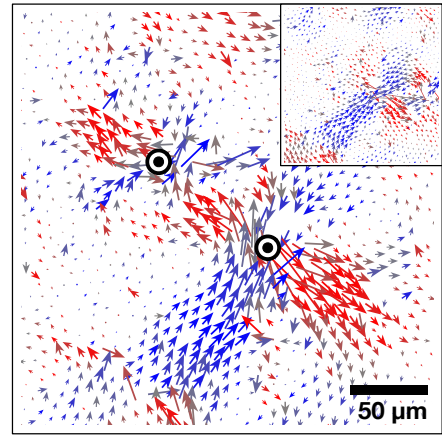


FIG. 1. **Experimental motivation.** Displacements of particles in a 2D amorphous solid experiment [22], showing rearrangements at two soft spots triggered by horizontal shear. The center of each rearrangement is marked with \otimes ; each has an extended quadrupolar displacement field (red and blue vectors, colored by direction). These fields conflict in the middle, suggesting a frustrated interaction. Inset: At other times, only one soft spot is rearranged. Details of experiments are in the Supplemental Materials [23].

of hysterons without interactions or with only “cooperative” interactions—in which one rearrangement facilitates another—reproduces the return-point memory behavior of some non-glassy systems [1, 7, 9, 28]. Switching the driving from typical symmetric cycles (positive and negative shear strain) to asymmetric (positive strain only) dramatically limits memory to a single amplitude. The picture changes for frustrated interactions in which one rearrangement inhibits another, observed in amorphous solids (Fig. 1) [11, 12, 14, 19, 29]. For symmetric driving the effect is perturbative, but under asymmetric driving it becomes dominant, allowing a clean measurement of information that could not be retained without frustration. We make sense of our results by showing that a frustrated pair of soft spots under asymmetric driving can be equivalent to a single non-interacting soft spot

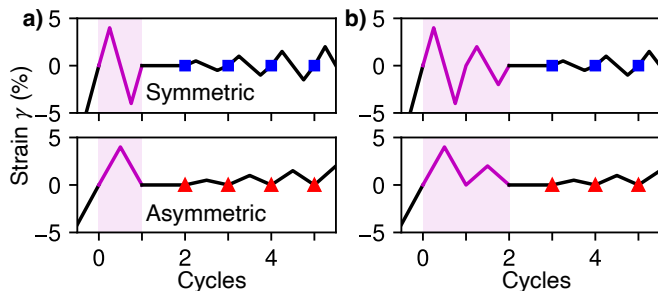


FIG. 2. **Driving protocols.** Write cycle(s) (magenta) and the first several cycles of readout (black) for (a) a single memory of strain 4% and (b) two memories at 4% and 2%. At the end of the write cycle(s), the system is in state S_{mem} , which is compared with the state at the end of each readout cycle (symbols).

under symmetric driving. Finally, we outline how this memory effect leads to design rules and to experimental tests of frustration that have otherwise been elusive.

Model — We are motivated by experiments and molecular dynamics simulations with amorphous solids in oscillatory shear, wherein groups of particles, sometimes identified as soft spots or shear transformation zones, can reversibly rearrange between two states under an imposed shear strain γ (Fig. 1). Modeling soft spots as discrete units that interact [19, 27, 29]—here, “hysterons”—captures many mesoscopic details of these studies [14, 19–21]. The i th hysteron switches its state S_i at thresholds γ_i^\pm : when $\gamma > \gamma_i^+$, $S_i = +1$; when $\gamma < \gamma_i^-$, $S_i = -1$; and when $\gamma_i^- < \gamma < \gamma_i^+$, S_i remains in its previous state. For convenience we write states as “+” and “−”. We simulate many systems of N hysterons with random parameters, modeling interactions via perturbed thresholds

$$\gamma_i^\pm(S_{j \neq i}) = \gamma_i^\pm - \sum_{j \neq i} J_{ij} S_j \quad (1)$$

where $S_{j \neq i}$ represents the states of all hysterons excluding hysteron i , and J_{ij} is the $N \times N$ interaction matrix. This is equivalent to the model in Ref. [12]. $J_{ij} < 0$ represents a frustrated interaction, where one hysteron flip inhibits another from flipping. We choose J_{ij} with uniform probability from $[-J_0, 0]$, with $J_0 = 0.01$ unless otherwise specified. Each hysteron’s γ_i^\pm are chosen by drawing two values from a uniform distribution on $[-0.1, 0.1]$, and then ordering them so that $\gamma_i^- < \gamma_i^+$, corresponding to rearrangements that dissipate energy.

Results — Protocols for initializing each simulation and writing and reading memories are shown in Fig. 2. We begin each simulation with all hysterons in the “−” state, as though $\gamma \rightarrow -\infty$, and then we drive the system to $\gamma = 0$ before encoding memories. (Starting at $\gamma \rightarrow \infty$ similarly supports our conclusions; it is considered in the Supplemental Materials [23].) Simulations used the open-

source **hysteron** software package [12]. Like molecular dynamics simulations, we work in the athermal and quasistatic limit: the algorithm identifies the hysteron that will flip soonest as γ changes, and then holds γ fixed while it updates any other hysterons that were destabilized via interactions (e.g. an avalanche), starting with the hysteron farthest past its threshold. When $N > 2$, a system’s parameters would occasionally prevent the algorithm from finding a stable state; these systems were discarded [12]. We did not consider systems where J_{ij} and J_{ji} have opposite signs, for which this issue is common.

After the writing cycle(s), the state is saved as S_{mem} . Without loss of generality, we take the single stored strain amplitude to be 4%, and in two-memory tests we use 4% and 2%. To read out the memories encoded in S_{mem} , we apply a series of cycles with increasing amplitude $\gamma_{\text{read}} = 0, 0.005, 0.01 \dots$. This is a “serial” protocol that is suited to experiments, as opposed to a “parallel” protocol in which a separate copy of the system is made for each readout cycle [30]. After each cycle with amplitude γ_{read} , we record the fraction of hysterons that are different from S_{mem} . We average this fraction over the entire ensemble of systems and plot it against γ_{read} .

Figure 3a shows readouts from the symmetric protocol in Fig. 2a. The curve from an ensemble of non-interacting hysterons ($J_{ij} = 0$) features a local minimum that indicates the memory, just as in the corresponding results from experiments and molecular dynamics simulations [18, 20, 22, 30]. However, in Fig. 3b driving the same ensemble asymmetrically changes its behavior dramatically: the curve is zero until the remembered value, past which it rises rapidly, reminiscent of memory in sheared dilute suspensions [4, 5, 31].

These strikingly different behaviors are expected from return-point memory, wherein the system remembers the turning points of driving. As long as γ is bounded between any pair of turning points, visiting either turning point will restore the system to its previous state when it was at that turning point [7, 9]. In Fig. 2a, the asymmetric protocol after initialization is bounded by 0 and 4%, and each readout cycle ends at $\gamma = 0$. Thus in Fig. 3b, without interactions, readout fails to change the system until $\gamma = 4\%$ is exceeded. By contrast, the corresponding curve in Fig. 3a has non-zero difference for $0 < \gamma_{\text{read}} < 4\%$ because each cycle has different turning points. Our results are consistent with the proof by Sethna et al. [9] that a system of hysterons with no interactions [7, 28] or cooperative interactions ($J_{ij} \geq 0$) must have return-point memory.

Figure 4a shows one hysteron’s response to symmetric writing and readout. Only hysterons such as this one, with $-\gamma^- > \gamma^+ > 0$, contribute to readout for $\gamma_{\text{read}} \leq 4\%$ because only they will be in the − state after training but become trapped in the + state upon reducing amplitude. From the distributions of γ^\pm , this

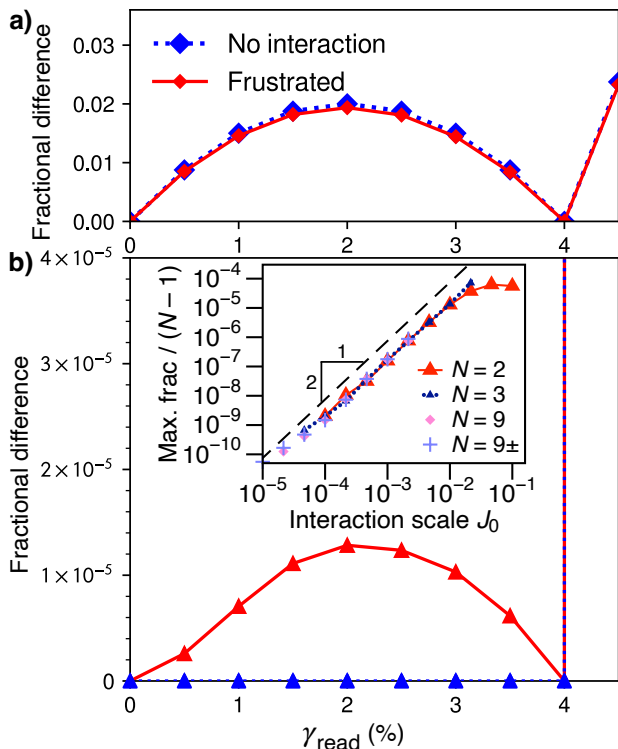


FIG. 3. **Readouts for memory of strain amplitude 4%**, in ensembles of 2×10^8 non-interacting hysterons, and of 10^8 $N = 2$ pairs with frustrated interactions. **(a)** Symmetric driving. Local minima indicate the memory. **(b)** Asymmetric driving. The curve without interactions is zero for $\gamma_{\text{read}} \leq 4\%$ and then increases, while the curve with frustration is non-monotonic. *Inset*: Maximum fractional difference for $\gamma_{\text{read}} < 4\%$ for various system sizes N and interaction scales J_0 , scaled by the number of pair interactions per hysteron $(N - 1)$. In “ $9\pm$,” half of the J_{ij}, J_{ji} pairs are positive (cooperative), so data are scaled by $(N - 1)/2$. Each point represents 10^9 systems. Dashed line shows J_0^2 scaling for reference.

mechanism yields the smooth curve in Fig. 3a.

Turning to glassy matter, we consider the effect of frustrated interactions in Fig. 3, $J_{ij} < 0$. These interactions generally mean that the sequences in which soft spots switch during forward or reverse shear can depend on history, leading to imperfect return-point memory [9, 13, 14, 16]. The effect on symmetric driving is perturbative, but the readout curve for asymmetric driving now resembles the much larger signal from symmetric driving, suggesting a connection.

The mechanism that creates this non-zero readout, shown in Fig. 4b, allows an asymmetrically-driven pair of hysterons with a frustrated interaction to mimic the single hysteron in Fig. 4a under symmetric driving. In this case, frustration allows a “latching” behavior in which revisiting the turning point at $\gamma = 0$ fails to restore the previous state.

What features are needed for latching? The values

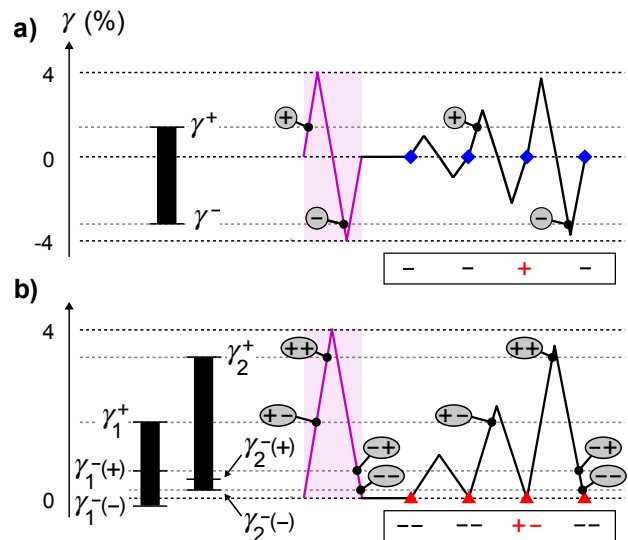


FIG. 4. **Hysteron systems that give rise to non-zero readout below the remembered strain.** Each schematic shows hysteron thresholds on the left and an abridged driving protocol on the right (colors as in Fig. 2). **(a)** Symmetric readout for a single hysteron. Changes in state during readout are indicated as plus and minus signs. State at the end of each cycle is shown below; nonzero readout (change in state) is in red. **(b)** Asymmetric readout for a frustrated pair. For clarity, we show only how the interaction splits the hysteron bottoms γ_1^- and γ_2^- as a function of the other hysteron’s state since the ordering of these four values is crucial for non-zero readout. The hysteron tops γ_1^+ and γ_2^+ can vary widely; see [23] for details.

γ_1^+ and γ_2^+ set the system’s sensitivity to amplitude; as long as they exceed most lower thresholds they can vary widely, creating the smooth, slightly asymmetric curves in Fig. 3b. By contrast, the lower thresholds must satisfy

$$\gamma_1^-(-) < 0 < \gamma_2^-(-) < \gamma_2^-(+) < \gamma_1^-(+), \quad (2)$$

as in Fig. 4b. These inequalities were verified in simulations by testing 10^9 random pairs. In the Supplemental Materials [23] we discuss the equivalent requirements in terms of transitions between states, and the case with $J_{21} > 0$, which relaxes $\gamma_2^-(-) < \gamma_2^-(+)$.

The interaction strength sets the threshold “window” size $\gamma_1^-(-) - \gamma_1^-(-) = -2J_{12}$. For a random frustrated pair to satisfy Eq. 2, both 0 and the interval $[\gamma_2^-(-), \gamma_2^-(+)]$ must fall in this window, limiting the probability for Eq. 2 and making it second-order in the interaction strength, i.e. $P \sim J_0^2$ for our simulations. The signals in Fig. 3b are thus small compared to the result from return-point memory under symmetric driving, which is zeroth-order in the sense that it may be obtained with $J_0 = 0$. The J_0^2 scaling is confirmed for small interaction strength ($J_0 \ll 4\%$) in the inset of Fig. 3b, where we measure the maximum height of the readout signal for $\gamma_{\text{read}} < 4\%$ [23].

The scaling estimate presented above is a departure from analyses of P based solely on the ordering of thresholds, as considered by van Hecke [13]: here we included the turning point of asymmetric driving, which additionally isolates the J_0^2 behavior by cutting out the zeroth-order response. Choice of driving protocol is thus a powerful tool for selecting terms in the readout signal.

The inset of Fig. 3b shows nearly identical results for larger systems after dividing out the multiplicity of frustrated pairs, even when we randomly make half of the interactions cooperative (drawn from $[0, J_0]$)—strongly suggesting that Fig. 4b is the dominant mechanism despite many more possible behaviors [11–14]. In the Supplemental Materials [23] we further show that the memory-forming portions of larger systems tend to have the same kinematics and interaction strengths as in $N = 2$. This remarkable conservation is possible because hysterons that do *not* contribute to asymmetric readout are largely following return-point memory, and so their states and transitions vary little from cycle to cycle.

We further illustrate this mechanism by the readout of multiple memories. Return-point memory is recursive, meaning that one may encode additional memories with a *symmetric* driving protocol by decreasing the strain amplitude, such that each new pair of turning points is nested within the last as in Fig. 2b. This is possible for the mechanism in Fig. 4a, where a subsequent cycle with a sufficiently small amplitude makes no change. Thus, of the hysterons that encode a memory from a 4%-amplitude writing cycle, some fraction will be undisturbed by writing and reading a memory of 2% and will retain the larger memory—while others will have the necessary thresholds to form and recall the memory of 2%, so that both memories appear during readout. This is seen in Fig. 5a, consistent with symmetrically-driven molecular dynamics simulations and experiments [18, 20, 22, 30]. However, return-point memory also means that two *asymmetric* cycles can write only one memory: the first cycle establishes a bounding turning point at $\gamma = 0$, and visiting $\gamma = 0$ again after writing the second, smaller amplitude immediately restores the state with just one memory (Fig. 5b).

The frustrated hysteron pair in Fig. 4b is also unchanged by small-amplitude cycles, suggesting that an ensemble can store nested memories of asymmetric driving. Indeed, in Fig. 5b frustrated interactions have restored the capacity for multiple memories. In the Supplemental Materials [23] we confirm that this capacity can be large, similar to return-point memory [7, 22, 32].

Discussion — Even though frustrated interactions are essential to the physics of amorphous solids [27, 33], crumpled sheets [15], and some magnetic systems [10, 16, 17] and mechanical metamaterials [34], in existing studies the response of glassy matter to symmetric driving tends to be dominated by hysteresis in the form of return-point memory, and the perturbative effects of frustration can

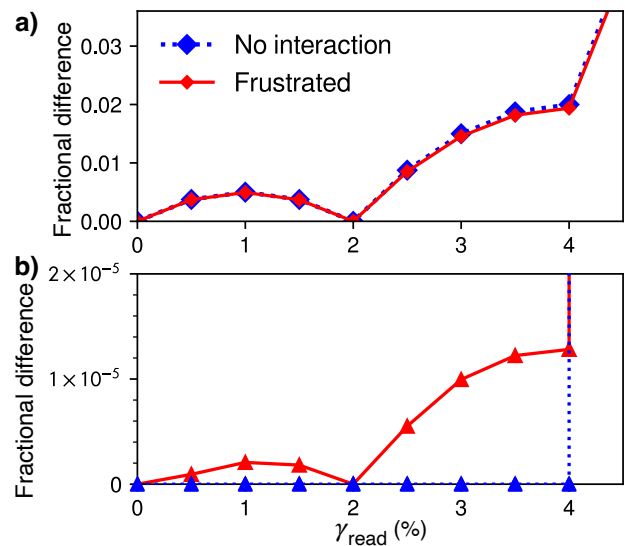


FIG. 5. **Readouts after writing memories at 4% and 2%.** (a) Curves from symmetric driving have cusps at 2% and 4%. (b) Asymmetric driving. Without interactions, only the memory at 4% is present. Curve from 10^8 frustrated pairs shows both memories.

be challenging to observe and understand. Our results show that a simple change to the driving protocol can suppress return-point memory to reveal a distinct memory behavior due to frustration. By considering each cycle as a transition to a new state [35], we identified the core mechanism in each scenario. These mechanisms can be embedded within larger systems, and they offer design rules for responding to a particular sequence of forcing [36], as in a single-dial combination lock [1].

It is helpful to view our results in terms of memory capacity—roughly, the number of possible histories that a system can distinguish. This question motivated previous studies of memory in artificial neural networks [37], self-assembling colloids [38], and dilute suspensions [4, 5, 35]. Because return-point memories can be nested, under symmetric driving the capacity of an amorphous solid can be large [18, 20, 22, 30, 32, 39]; here we add to the evidence that breaking return-point memory can allow for even greater capacity, as also suggested by studies of glassy systems that consider the ability to count repeated cycles [11–14].

Because the signal is dominated by a single mechanism for small interaction strengths even in large systems, this memory of asymmetric driving is also appropriate for experiments that seek signs of frustration in amorphous solids and other glassy athermal matter. Experiments and molecular dynamics simulations can test our results and characterize interaction strengths, by tracking individual relaxations while varying the amplitude and origin of asymmetric driving. More generally, the readout method is based on differences, and so we look forward to results like those in Fig. 5b that quantify frustration in

macroscopic samples via measurements of magnetization, light scattering, or even image subtraction [22].

We thank Martin van Hecke for insightful conversations. CWL was supported by the US Department of Energy, Office of Science, Basic Energy Sciences, under Grant DE-SC0020972. TRJ was supported in part by a Remote Innovation Grant from the Student Engagement Network at Penn State, and by a grant from the Schreyer Honors College at Penn State.

* cwindeman@uchicago.edu

† travisj@uoregon.edu; Knight Campus, University of Oregon, Eugene, OR, USA

‡ keim@psu.edu

- [1] N. C. Keim, J. D. Paulsen, Z. Zeravcic, S. Sastry, and S. R. Nagel, *Rev. Mod. Phys.* **91** (2019).
- [2] L. Mullins, *Rubber Chem. and Tech.* **42**, 339 (1969).
- [3] J. Kaiser, Doctoral Thesis, Tech. Hosch, Munich (1950).
- [4] N. C. Keim and S. R. Nagel, *Phys. Rev. Lett.* **107** (2011).
- [5] J. D. Paulsen, N. C. Keim, and S. R. Nagel, *Phys. Rev. Lett.* **113** (2014).
- [6] S. N. Coppersmith, T. C. Jones, L. P. Kadanoff, A. Levine, J. P. McCarten, S. R. Nagel, S. C. Venkataramani, and X. Wu, *Phys. Rev. Lett.* **78**, 3983 (1997).
- [7] J. Barker, D. Schreiber, B. Huth, and D. H. Everett, *Proc. Roy. Soc. A* **386**, 251–261 (1983).
- [8] P. H. Emmett and M. Cines, *J. Phys. Chem.* **51**, 1248–1262 (1947).
- [9] J. P. Sethna, K. Dahmen, S. Kartha, J. A. Krumhansl, B. W. Roberts, and J. D. Shore, *Phys. Rev. Lett.* **70**, 3347 (1993).
- [10] K. Binder and A. P. Young, *Rev. Mod. Phys.* **58**, 801 (1986).
- [11] C. Lindeman and S. Nagel, *Sci. Adv.* **7**, eabg7133 (2021).
- [12] N. C. Keim and J. D. Paulsen, *Sci. Adv.* **7** (2021).
- [13] M. van Hecke, *Phys. Rev. E* **104**, 054608 (2021).
- [14] A. Szulc, M. Mungan, and I. Regev, *J. Chem. Phys.* **156**, 164506 (2022).
- [15] D. Shohat, D. Hexner, and Y. Lahini, *Proc. Nat. Acad. Sci.* **119** (2022).
- [16] O. Hovorka and G. Friedman, *J. Magn. Magn. Mater.* **290**, 449–455 (2005).
- [17] I. Gilbert, G.-W. Chern, B. Fore, Y. Lao, S. Zhang, C. Nisoli, and P. Schiffer, *Phys. Rev. B* **92**, 104417 (2015).
- [18] D. Fiocco, G. Foffi, and S. Sastry, *Phys. Rev. Lett.* **112** (2014).
- [19] M. Mungan, S. Sastry, K. Dahmen, and I. Regev, *Phys. Rev. Lett.* **123** (2019).
- [20] N. C. Keim, J. Hass, B. Kroger, and D. Wieker, *Phys. Rev. Research* **2** (2020).
- [21] I. Regev, I. Attia, K. Dahmen, S. Sastry, and M. Mungan, *Phys. Rev. E* **103**, 062614 (2021).
- [22] N. C. Keim and D. Medina, *Sci. Adv.* **8**, eabo1614 (2022).
- [23] See Supplemental Material at [URL] for details about the experimental figure, the role of system initialization, and the role of interaction strength scales; and analyses of relevant $N = 2$ transition graphs, memory in larger systems, and memory capacity.
- [24] M. L. Falk and J. S. Langer, *Ann. Rev. Cond. Mat. Phys.* **2**, 353–373 (2011).
- [25] M. L. Manning and A. J. Liu, *Phys. Rev. Lett.* **107**, 108302 (2011).
- [26] E. D. Cubuk, R. J. S. Ivancic, S. S. Schoenholz, D. J. Strickland, A. Basu, Z. S. Davidson, J. Fontaine, J. L. Hor, Y. R. Huang, Y. Jiang, N. C. Keim, K. D. Koshigan, J. A. Lefever, T. Liu, X. G. Ma, D. J. Magagnosc, E. Morrow, C. P. Ortiz, J. M. Rieser, A. Shavit, T. Still, Y. Xu, Y. Zhang, K. N. Nordstrom, P. E. Arratia, R. W. Carpick, D. J. Durian, Z. Fakhraai, D. J. Jerolmack, D. Lee, J. Li, R. Riggleman, K. T. Turner, A. G. Yodh, D. S. Gianola, and A. J. Liu, *Science* **358**, 1033–1037 (2017).
- [27] A. Nicolas, E. E. Ferrero, K. Martens, and J.-L. Barrat, *Rev. Mod. Phys.* **90**, 341–363 (2018).
- [28] F. Preisach, *Zeitschrift für Physik* **94**, 277 (1935).
- [29] K. Khirallah, B. Tyukodi, D. Vandembroucq, and C. E. Maloney, *Phys. Rev. Lett.* **126**, 218005 (2021).
- [30] M. Adhikari and S. Sastry, *Eur. Phys. J. E* **41**, 045504 (2018).
- [31] N. C. Keim, J. D. Paulsen, and S. R. Nagel, *Phys. Rev. E* **88** (2013).
- [32] I. Regev, I. Attia, K. Dahmen, S. Sastry, and M. Mungan, *Phys. Rev. E* **103**, 062614 (2021).
- [33] D. Kumar, S. Patinet, C. Maloney, I. Regev, D. Vandembroucq, and M. Mungan, *J. Chem. Phys.* **157**, 174504 (2022).
- [34] C. Merrigan, C. Nisoli, and Y. Shokef, *Phys. Rev. Research* **3** (2021).
- [35] J. D. Paulsen and N. C. Keim, *Proc. Roy. Soc. A* **475**, 20180874 (2019).
- [36] J. Ding and M. van Hecke, *The Journal of Chemical Physics* **156**, 204902 (2022).
- [37] J. J. Hopfield, *Proc. Nat. Acad. Sci.* **79**, 2554 (1982).
- [38] A. Murugan, Z. Zeravcic, M. P. Brenner, and S. Leibler, *Proc. Nat. Acad. Sci.* **112**, 54 (2015).
- [39] S. Mukherji, N. Kandula, A. K. Sood, and R. Ganapathy, *Phys. Rev. Lett.* **122**, 158001 (2019).

Supplementary Material for “Isolating the Enhanced Memory of a Glassy System”

(Dated: November 14, 2023)

I. DETAILS FOR FIGURE 1

Experimental particle trajectories for Fig. 1 were obtained using methods and materials described in Ref. [1]. We cyclically sheared a monolayer of bidisperse polystyrene particles adsorbed at an oil-water interface. These adsorbed particles have an electrostatic dipole-dipole repulsion, so that the material is a disordered, frictionless soft solid.

The displacements in Fig. 1 are computed by tracking particles [2] and comparing their positions during forward and reverse shear at the same value of strain, within a single cycle of strain amplitude $\gamma_0 = 4.7\%$. The same method and trajectory data were the basis for the analyses of Fig. 5 of Ref. [1]. The main plot in Fig. 1 is from samples at $\gamma = 2.00\%$, and the inset corresponds to $\gamma = -0.72\%$.

In each plot, we subtract the average motion of the region of surrounding material with radius $12.5a$, where a is the mode of the interparticle distance, determined from the pair correlation function $g(r)$ [3–5]. We also remove 1–3 particles in each plot that showed large displacements despite being far from the core of each rearrangement, due to particle tracking errors. We identified these errant particles as having displacements ≥ 5 times larger than the median displacement magnitude of their neighbors, within a radius $2.5a$.

II. EFFECT OF INITIAL CONDITION

In the main text we consider asymmetric driving with positive strain only, and all hysteros beginning in the “–” state—opposite the polarity of driving, as shown in Fig. 2. Here we describe simulations that begin in the “+” state, as though $\gamma \rightarrow \infty$; in these simulations we drive the system to $\gamma = 0$ and then write and read memories as in Fig. 2. Figure S1 shows these results along with the curves from Figs. 3 and 5. The effect on *symmetric* driving in Fig. S1(a, c) is subtle. However, the effect of initialization on return-point memory under *asymmetric* driving in Fig. S1(b, d) can be dramatic. In simulations without interactions ($J_{ij} = 0$) the asymmetric curve initialized with same (positive) sign shows no memory at all—it has a fractional difference of 0 for all readout strains. This is a consequence of return-point memory: because γ is bounded between ∞ and 0, visiting the turning point at 0 after each cycle restores the system to its state before encoding. By contrast, the second-order memory mechanism illustrated in Fig. 4b is not return-point memory, and its behavior for $\gamma \leq 4\%$ is the same whether we first approach $\gamma = 0$ from $+\infty$ or $-\infty$. Thus in Fig. S1b, the two asymmetric protocols each form a memory, and their readout results agree for $\gamma_{\text{read}} < 4\%$. Differences at larger γ_{read} are due to hysteros that were not affected by writing and readout, and that retain only a memory of the initial condition.

Asymmetric driving with same-polarity initialization is thus a special case for return-point memory, and for simplicity we have omitted it from the main text. Other initialization protocols [1] will generally be able to form memories of single amplitudes under asymmetric driving, even in systems with perfect return-point memory. We note that the readout behavior past the stored memory (here, at $\gamma_{\text{read}} = 4\%$) is itself a kind of memory of initial conditions.

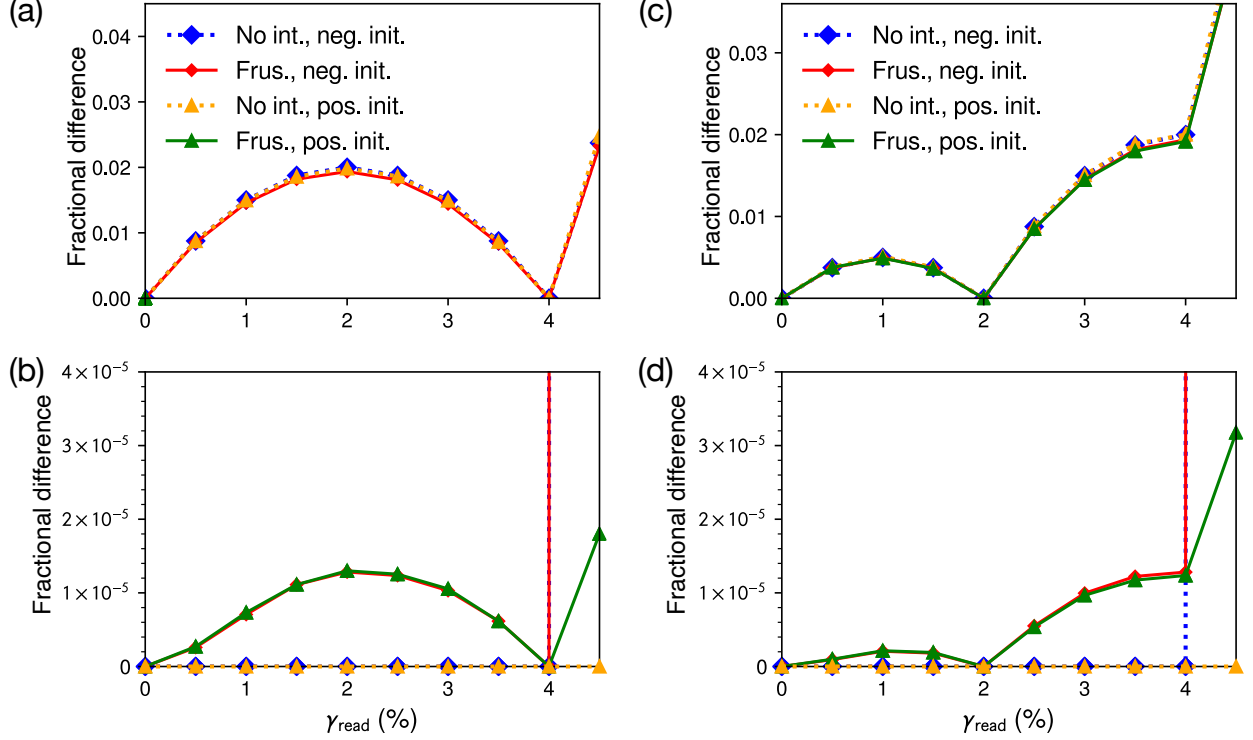


FIG. S1. **Readout curves showing role of initialization for asymmetric driving.** Data are reproduced from Figs. 3 and 5, with the addition of frustrated systems starting from an all-positive initial state (i.e. the same polarity as driving). (a) Readouts after writing a single memory at $\gamma = 4\%$. (b) Readouts after writing memories at 4% and 2%. Positive initialization has no effect on the two-hysteron mechanism that gives rise to the signal for $\gamma_{\text{read}} \leq 4\%$, while it changes the slope of the response at larger γ_{read} .

III. INTERACTION STRENGTH

There are three strain scales that play a role in the effect of interactions on a pair of hysterons: the amount of hysteresis before adding interactions $\gamma^+ - \gamma^-$ (sometimes called the hysteron length), the interaction strength scale J_0 , and the driving amplitude, taken here to be a few percent, $\gamma_0 \approx 0.04$. The effect of the driving amplitude is to select which hysterons are involved in the training and readout process: only hysterons with hysteresis $\gamma^+ - \gamma^- \sim \gamma_0$ can contribute. Here, the hysteresis is effectively chosen from $[0, 0.2]$, and the contributing hysterons are further cut down by $\gamma_0 \approx 0.04$. A natural non-dimensional scale of interaction strength would therefore be relative to the driving amplitude: $J^* \sim J_0/\gamma_0$. In our scaling study, J_0 ranges from 10^{-5} to 10^{-2} , giving J^* from $\sim 3 \times 10^{-4}$ to ~ 0.3 .

Note that in other cases where hysteresis is small relative to the driving amplitude, the non-dimensional scale of interaction strength might be better defined as the ratio of J_0 to the hysteron length.

IV. READOUT CURVES FOR VARIOUS J_0 AND N

Figure S2 shows the readout curves, generated in the manner of Fig. 3b, that were used to measure memory signal strength for the inset of Fig. 3b. The “maximum memory signal” plotted

in the inset of Fig. 3b refers to the maximum value of each curve for $\gamma_{\text{read}} < 4\%$, and is measured only on curves that are non-monotonic, meaning that some larger values of J_0 are not plotted in the paper. We also omit measurements for $N = 2$, $J_0 < 10^{-4}$, for $N = 3$, $J_0 < 4.6 \times 10^{-5}$, and for $N = 9$, $J_0 < 2.2 \times 10^{-5}$ because in those cases the entire signal comes from at most 1 hysteron, making a measurement difficult to interpret.

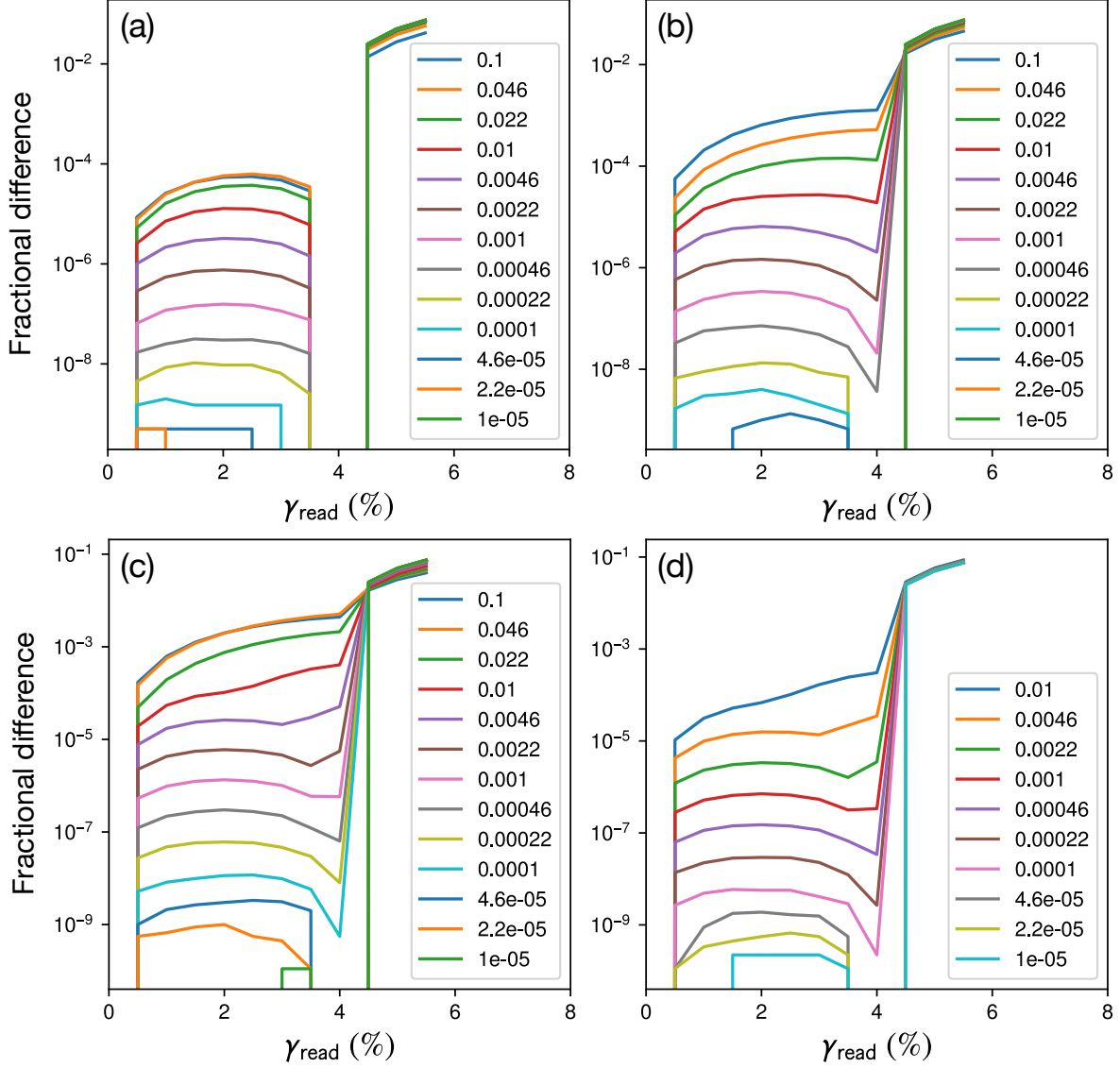


FIG. S2. **Single-memory readout curves for various interaction strength scales J_0 and system size N .** Each panel corresponds to a curve in the inset of Fig. 3b: (a) $N = 2$; (b) $N = 3$; (c) $N = 9$; (d) the “ $N = 9\pm$ ” case where J_{ij}, J_{ji} pairs are made positive with probability $1/2$. The legend identifies the value of J_0 for each curve and matches the vertical order of the curves; larger J_0 generally result in larger fractional differences. Fractional differences of zero are not shown on these logarithmic axes. Each curve was generated from an ensemble of 10^9 systems, with the same asymmetric protocol in Fig. 2a that was used for the main panel of Fig. 3b.

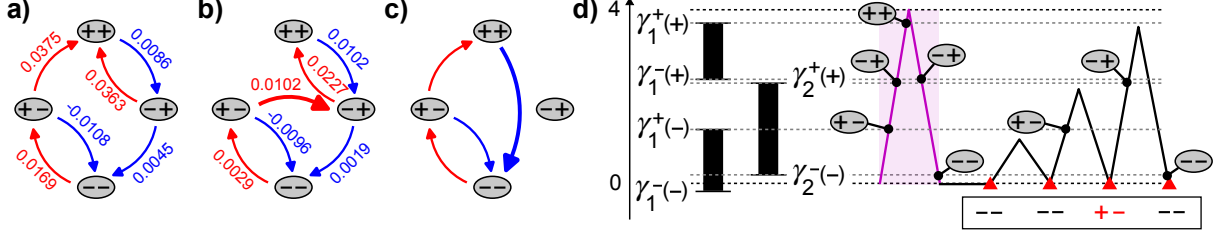


FIG. S3. **Two-hysteron transition graphs that give rise to non-zero readout below the remembered strain.** Transitions encountered upon increasing (decreasing) strain are in red (blue). Examples of strain values that give rise to such a behavior are shown. (a) Transition graph corresponding to the example in Fig. 4b. (b) A second contributing transition graph, which occurs when $\gamma_1^-(+) > \gamma_2^+(+)$. This causes a so-called “horizontal” avalanche when the second hysteron flips to the + state under increasing strain [6]. (c) A third contributing transition graph, which occurs when $\gamma_2^-(-) > \gamma_1^+(+)$. This causes a so-called “vertical” avalanche when the first hysteron flips to the – state under decreasing strain. No example strains are given because strictly negative interactions in the $N = 2$ systems simulated prevented such a graph from contributing to readout. (d) Example hysterons in the strain-space format of Fig. 4 of the main text and corresponding to the type of transition graph shown in (b) (the flipping strains shown are not the exact values marked in (b); rearrangements have been spaced out for clarity).

V. TRANSITION GRAPHS AND GENERALIZED INEQUALITIES

A particular hysteron system can be represented as a transition graph, in which nodes are states of the system (for example, ++ or +-) and arrows represent transitions between states for increasing and decreasing strain. For two hysterons, all such transition graphs are enumerated in [6]. Of those, only three contribute to the non-zero readout signal explored in Fig. 4. These transition graphs are shown in Fig. S3, with example values of the flipping strains given for each arrow in the cases observed in simulation. These example flipping strains satisfy Eq. 2.

Note that, in practice, the transition graph in Fig. S3b did not contribute substantially to the readout signals, as it requires large interaction strength relative to the length $\gamma_2^+ - \gamma_2^-$ of hysteron 2. We quantify this contribution in the bottom row of Table S1. The transition graph in Fig. S3c did not contribute at all because it requires breaking the rule used throughout the main text that each J_{ij}, J_{ji} pair must have the same sign [6].

To generalize the inequalities in Eq. 2 of the main text to include all three transition graphs, we allow for non-frustrated interactions. For the latching mechanism necessary for non-zero readout to occur, we still need one frustrated interaction (without loss of generality, $J_{12} < 0$), so the only new case allowed by this relaxation of strictly frustrated interactions is $J_{21} > 0$.

The general picture that emerges from the three contributing diagrams (shown in Fig. S3a-c) is (1) that the system must travel through all four states in a cycle of sufficient size (rather than, for example, going through +- on both the way up and the way down); and (2) that the transition back from +- to -- is outside the range of driving, that is, below zero. This sets up the following inequalities:

- If we define hysteron 1 as the hysteron that flips forward first, then hysteron 1 should also be the first to flip back: $\gamma_1^-(+) > \gamma_2^-(+)$. This makes it possible to travel through all four states in a shear cycle.
- The transitions from ++ to +- and from +- to -- must occur at $\gamma > 0$. In other words, since we have already determined that hysteron 1 is the first to flip back to -, $\gamma_1^-(+) > 0$ and $\gamma_2^-(-) > 0$.

	N	2	3	9	$9\pm$ (a)	$9\pm$ (b)
$P(\text{coop})$		0	0	0	1/2	1/2
J_0		1.00×10^{-2}	2.00×10^{-3}	2.00×10^{-3}	2.00×10^{-3}	1.00×10^{-2}
$P(\text{sig})$		2.07×10^{-5}	2.19×10^{-6}	8.71×10^{-6}	4.72×10^{-6}	7.82×10^{-5}
$P(\text{sig})/(N-1)(1-P(\text{coop}))J_0^2$		0.21	0.27	0.27	0.30	0.20
$P(\text{kine} \mid \text{sig})$		1	0.98	0.91	0.82	0.67
$P(\text{param} \mid \text{kine})$		1	0.24	7.21×10^{-2}	4.57×10^{-2}	4.69×10^{-2}
$P(\text{coop} \mid \text{kine})$					1.22×10^{-2}	6.09×10^{-2}
$\langle J_{12} \rangle / J_0$		-0.78	-0.80	-0.80	-0.79	-0.77
$\langle J_{21} \rangle / J_0$		-0.18	-0.20	-0.20	-0.21	-0.20
$P(\text{avalanche} \mid \text{kine})$		2.24×10^{-2}	0	0	0	2.20×10^{-2}

TABLE S1. **The pair mechanism of Fig. 4b dominates memory of asymmetric driving in larger systems.** Analysis was performed on ensembles of 10^9 systems of size N (columns); for the two “ $9\pm$ ” ensembles, pairs of J_{ij}, J_{ji} were made positive with probability 1/2. Analysis identified hysterons that contributed to the readout signal (“sig”), that matched the kinematics of Figs. 4b and/or S3d (“kine”), and that had cooperative interactions (“coop”) or horizontal avalanches as in Fig. S3d (“avalanche”). $P(\text{sig})$ is also rescaled according to inset of Fig. 3b. Average interaction values $\langle J_{12} \rangle, \langle J_{21} \rangle$ are from hysteron pairs that match kinematics and have a frustrated interaction; subscripts refer to the corresponding hysteron indices in Fig. 4b. $\langle J_{12} \rangle, \langle J_{21} \rangle$ are remarkably consistent, suggesting that memory kinematics of a pair are driven primarily by their interaction, even in larger systems.

- The transition from $+-$ to $--$ must be below zero: $\gamma_1^-(-) < 0$. This prevents the system from always returning to the same state when the strain is returned to 0.

More concisely, the necessary and sufficient set of inequalities to get non-zero readout below the training strain for two interacting hysterons that have been driven asymmetrically is

$$\gamma_1^-(-) < 0 < \gamma_1^-(+); \gamma_2^-(+) < \gamma_1^-(+); 0 < \gamma_2^-(-), \quad (\text{S1})$$

which is satisfied by graphs S3(a-c) and in Figs. 4b and S3d, and of which Eq. 2 is the special case for $J_{21} < 0$.

VI. FRUSTRATED-PAIR MECHANISM IN LARGER SYSTEMS

The scaling analysis in Fig. 3b suggested that the memory of asymmetric driving in larger systems (Fig. S2) was dominated by the action of frustrated pairs. While for $N = 2$ one can predict memory behavior by inspecting a system’s parameters (Eqs. 1 and 2), in larger systems the numerous interactions and metastable states make this impractical. Instead, we can investigate the origins of memory readout signals in larger systems and ask whether the mechanism for memory in a pair is at work, by examining kinematics: the transitions of individual hysterons within larger systems, as a memory is written and read with the asymmetric protocol in Fig. 2a.

Table S1 summarizes our analysis of the kinematics in ensembles of 10^9 systems, generated according to the same schemes as the inset of Fig. 3b and Fig. S2. We fix the maximum interaction strength at $J_0 = 2 \times 10^{-3}$, except $J_0 = 10^{-2}$ for $N = 2$, when the memory behavior is least likely to occur in each system. We first drive an ensemble with the single-memory asymmetric protocol in Fig. 2a. We identify the probability $P(\text{sig})$ that a given hysteron contributes to a non-monotonic memory readout signal, as in Fig. 3b — specifically, that its state after the cycle with $\gamma_{\text{read}} = 4\%$ matches its state at the beginning of readout, and that it is in a different state at the end of at least one intervening cycle.

Next, each hysteron that counts toward $P(\text{sig})$ belongs to several interacting pairs (in our systems, $N - 1$ pairs). For each pair, we extract the sequence of states that the pair visits in each

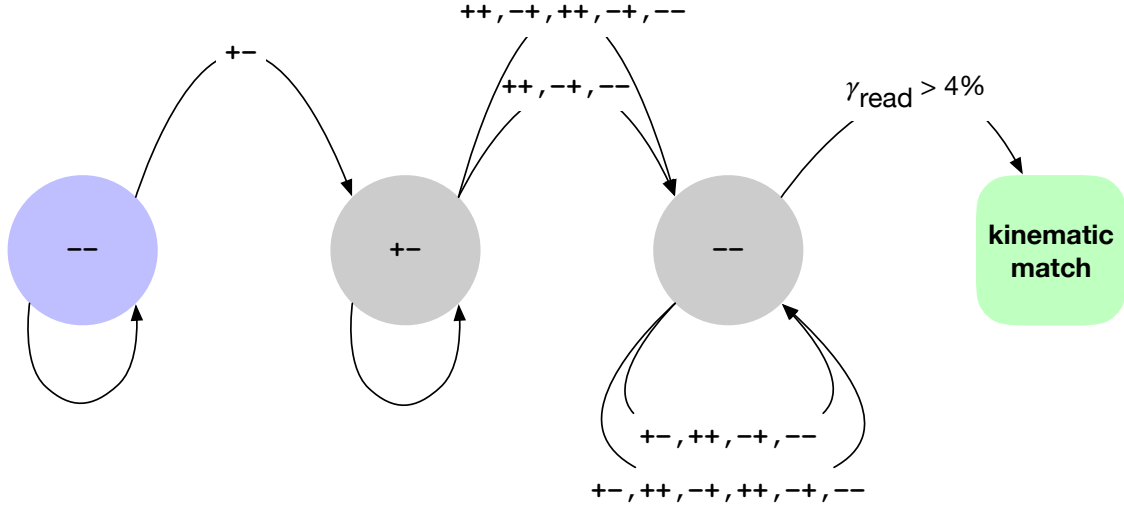


FIG. S4. **Testing the kinematics of a hysteron pair.** A finite-state machine tests whether the kinematics of a memory-encoding pair during readout match the readout sequence shown in Fig. 4b or Fig. S3d. Each arrow represents one cycle of asymmetric driving and shows the sequence of states (if any) during that cycle; each node represents the state at the beginning/end of the cycle. Readout begins in the $--$ state at left and proceeds with increasing γ_{read} . To be accepted as a kinematics match, a hysteron pair must follow only an allowed sequence of states, and must be in the right-hand $--$ state after the cycle with $\gamma_{\text{read}} = 4\%$ (the strain amplitude that was written). The longer sequences from $+-$ to $--$ and from $--$ to itself correspond to the uppermost transitions in Fig. S3b.

cycle of readout. Figure 4b establishes that the memory behavior of interest arises from the distinct sequences obtained during small-, medium-, and large- amplitude cycles. To check whether these sequences match the progressions in Fig. 4b or Fig. S3d, our analysis implements the finite-state machine in Fig. S4; this also checks for a (rare) variant made possible by the avalanche behavior. We then ask: of the hysterons that contribute to the readout signal, what fraction $P(\text{kine} \mid \text{sig})$ belongs to exactly one pair that matches these kinematics? Remarkably, in Table S1 we report that $P(\text{kine} \mid \text{sig}) \sim 1$ even in large systems with cooperative and frustrated interactions (“9 \pm ”).

We can further ask whether the actual mechanism of Fig. 4b, which is based on an isolated pair of hysterons, has any explanatory value for the pairs in larger systems. At one extreme, one might hypothesize that these pairs are nearly isolated from the rest of their systems, so that their randomly-generated interaction *and* threshold parameters are often consistent with Eq. 2—a probability we measure as $P(\text{param} \mid \text{kine})$. Instead, Table S1 shows that $P(\text{param} \mid \text{kine}) \ll 1$ in large systems, meaning that the effects of other hysterons on the thresholds in Eq. 2 are significant; the behavior cannot be predicted from the two hysterons alone.

At the other extreme, one might hypothesize that a pair of hysterons with memory kinematics is merely a “puppet” of other hysterons with unknown memory behaviors, and that the interaction within the pair is so unimportant that it need not even be frustrated. In the “9 \pm ” ensembles where cooperative interactions occur with probability 0.5, we find that this “puppet” scenario is not supported, since $P(\text{coop} \mid \text{kine}) \ll 1$.

Most remarkably, Table S1 shows that for hysteron pairs that match kinematics and have a frustrated interaction, the mean interaction values $\langle J_{12} \rangle, \langle J_{21} \rangle$ are nearly the same fraction of J_0 in all ensembles. In other words, the kinematics of a memory-forming pair within a larger system are driven by the interactions within that pair, in the same way as for $N = 2$. Together, the results in Table S1 strongly support our interpretation of the J_0^2 scaling results in the inset of Fig. 3b: the mechanism in Fig. 4b is the dominant way a system remembers asymmetric driving, even in large

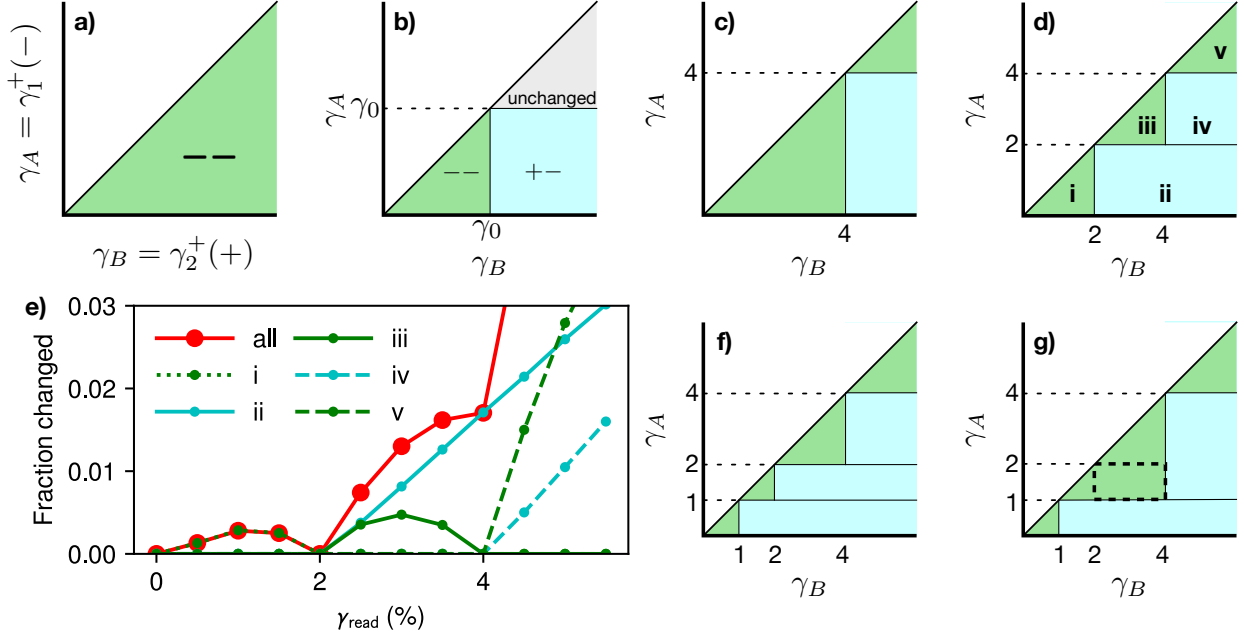


FIG. S5. **Graphical analysis of multiple memories.** Each pair of hysterons like Fig. 4b can be represented as a point on a plane, according to its upper thresholds. (a) An infinite ensemble of such pairs with continuously-distributed thresholds, all initialized to the $--$ state. The thresholds are labeled γ_A, γ_B for convenience. In accordance with Fig. 4b, $0 < \gamma_A < \gamma_B$. (b) “Template” for how an asymmetric cycle with amplitude γ_0 changes the states of pairs in the ensemble. (c) The ensemble in (a), after one cycle with amplitude 4% forms a memory. (d) The ensemble encodes two memories after cycles with 4% and 2% amplitude. (e) Readout of the ensemble in (d), reporting the fraction of hysterons in different states, as a fraction of all hysterons in pairs that conform to Fig. 4a or Fig. S3d. Curves show readout of all such pairs (“all”), and of ensembles generated separately to match each labeled region in (d). (f) Ensemble after cycles with 4%, 2%, and 1%. (g) Ensemble after cycles with 4% and 1%. Comparing with (f) reveals the set of pairs (outlined with heavy dashes) that encode the difference between these histories.

systems with a mixture of cooperative and frustrated interactions.

VII. GENERALIZING THE CAPACITY FOR MULTIPLE MEMORIES

As noted in the main text, the mechanism we identify for a hysteron pair is a way to store arbitrarily many memories of asymmetric driving. To see this in detail, we consider an infinite ensemble of frustrated pairs like Fig. 4b, with a continuous distribution of γ^+ . With interactions, the relevant upper thresholds in Fig. 4b and Fig. S3d are $\gamma_1^+(-)$, which we label γ_A for convenience, and $\gamma_2^+(+)$, which we label γ_B . In Fig. S5a we represent each pair in the ensemble as a point on the γ_B - γ_A plane, with $0 < \gamma_A < \gamma_B$ as required for our mechanism, and with all such pairs initialized in the $--$ state.

Figure 4b shows how the amplitude of driving γ_0 selects one of three possible outcomes for a given hysteron pair: the pair’s state is unchanged if $\gamma_0 < \gamma_A$, it becomes $+ -$ if $\gamma_A \leq \gamma_0 < \gamma_B$, and it becomes $--$ if $\gamma_0 \geq \gamma_B$. These outcomes correspond to three regions in Fig. S5b: pairs with $\gamma_B < \gamma_0$ are placed in the $--$ state, pairs with $\gamma_B > \gamma_0$ and $\gamma_A < \gamma_0$ are placed in $+ -$, and pairs with $\gamma_A > \gamma_0$ are undisturbed.

By applying this template to the plane repeatedly, we can find the state of the ensemble after an arbitrary sequence of amplitudes. For example, in Fig. S5(c, d) cycles of amplitude 4% and

then 2% write two memories, as in the protocol of Fig. 2b. To understand readout with cycles of increasing amplitude, we place the template at $\gamma_0 = 0$ and imagine sweeping it up and to the right. Pairs that begin readout as $--$ are changed to $+-$ as the leading (horizontal) edge of the template passes over them, and then changed back to $--$ by the trailing (vertical) edge. However, for pairs in the $+-$ state at the start of readout (due to memories), the leading edge has no effect, but the trailing edge changes them so that they contribute to the readout signal. The memories encoded on the $\gamma_B\text{-}\gamma_A$ plane thus modulate the readout signal and change its slope. We confirm this picture by repeating the readout simulation in Fig. 5b of the paper, but for sub-ensembles that conform to each of the demarcated regions in Fig. S5d in isolation. Each region’s distinct contribution to the readout signal is shown in Fig. S5e.

Figure 4 also showed a correspondence between our frustrated-pair mechanism for asymmetric driving, and the Preisach model of non-interacting hysterons for symmetric driving. Indeed, for symmetric driving that begins with positive strain, the change of variables $\gamma_A \rightarrow -\gamma^-$, $\gamma_B \rightarrow \gamma^+$ makes our arguments resemble analyses of return-point memory [1, 5, 7] based on the graphical representation introduced by Preisach [8].

Following the argument of Keim and Medina [1], we consider briefly the memory capacity of a finite ensemble of frustrated pairs. Figure S5f adds a third memory, and illustrates that nested memories form a stair-step pattern on the plot. If the density of hysteron pairs on the plane is finite, then these stair-steps can be subdivided only so many times before they become indistinct. More precisely, if we generalize our memory values as the descending sequence $\gamma_n, \gamma_{n-1}, \dots, \gamma_2, \gamma_1$, then memory $0 < m < n$ from within the sequence will be encoded by the pairs in the rectangle $\gamma_m < \gamma_B \leq \gamma_{m+1}$, $\gamma_{m-1} < \gamma_A \leq \gamma_m$. This can be seen by comparing Fig. S5f with the outcome if the 2% memory had not been written (Fig. S5g); the highlighted rectangle encodes this difference. If there is no pair of hysterons within such a rectangle, then the ensemble’s state will be the same whether γ_m was written or not—the memory capacity has been exceeded. Thus, in an ensemble of N pairs, the maximum number of distinct memories M scales as the maximum number of distinct rectangles that can be drawn in this way, such that each rectangle contains at least one pair. Since the area of each rectangle scales as $1/M^2$, we obtain $M \sim \sqrt{N}$ as in the Preisach model [1, 9]. The presence or absence of each memory corresponds to a different history, and so readout lets one distinguish among $\sim 2^M$ possible histories of asymmetric driving.

-
- [1] Nathan C. Keim and Dani Medina, “Mechanical annealing and memories in a disordered solid,” *Sci. Adv.* **8**, eabo1614 (2022).
 - [2] Daniel B. Allan, Thomas Caswell, Nathan C. Keim, and Casper M. van der Wel, “Trackpy v0.4.2,” DOI:10.5281/zenodo.3492186 (2019).
 - [3] Nathan C Keim and Paulo E Arratia, “Mechanical and microscopic properties of the reversible plastic regime in a 2d jammed material,” *Phys. Rev. Lett.* **112**, 028302 (2014).
 - [4] Nathan C Keim, “Philatracks v0.2,” DOI:10.5281/zenodo.11459 (2014).
 - [5] Nathan C. Keim, Jacob Hass, Brian Kroger, and Devin Wieker, “Global memory from local hysteresis in an amorphous solid,” *Phys. Rev. Research* **2** (2020).
 - [6] Martin van Hecke, “Profusion of transition pathways for interacting hysterons,” *Phys. Rev. E* **104**, 054608 (2021).
 - [7] J Barker, D Schreiber, BG Huth, and D H Everett, “Magnetic hysteresis and minor loops: Models and experiments,” *Proc. Roy. Soc. A* **386**, 251–261 (1983).
 - [8] F. Preisach, “Über die magnetische nachwirkung,” *Zeitschrift für Physik* **94**, 277–302 (1935).
 - [9] Ido Regev, Ido Attia, Karin Dahmen, Srikanth Sastry, and Muhittin Mungan, “Topology of the energy landscape of sheared amorphous solids and the irreversibility transition,” *Phys. Rev. E* **103**, 062614 (2021).